

NANO EXPRESS

Open Access

Morphology and property control of NiO nanostructures for supercapacitor applications

Farrukh Iqbal Dar, Kevin Radakishna Moonoswamy and Mohammed Es-Souni*

Abstract

We process one-dimensional (1D) NiO nanostructures in anodized alumina templates starting from electrochemically deposited Ni nanotubes (NTs), and characterize their morphology-dependent supercapacitance behavior. The morphology of the 1D NiO nanostructures is controlled by the time of annealing at 450°C. After 25 min of annealing, the NTs start to close but maintain the tubular structure, and after a further 300 min of annealing time, the tubes are completely closed and nanorods (NRs) are formed. We show that the structures obtained are highly promising for supercapacitor applications; the performance of the NiO NT structure is with a specific capacitance of 2,093 F/g, the highest ever obtained for NiO, approaching the theoretical capacitance of this material. A suitable combination of nanocrystalline grain size and the high surface area akin to the tubular structure is responsible for this high performance. In contrast, the NiO NR structure is characterized by lower performance (797 F/g). A further attribute of the proposed structure is its high stability against galvanostatic charging-discharging cycling at high current densities, with almost no alteration to performance after 500 cycles.

Keywords: NiO nanostructures; AAO-aided template synthesis; Electrodeposition; Supercapacitor

Background

Electrochemical capacitors that are also designated supercapacitors [1] derive their energy storage capacity from interaction between electrode and electrolyte at the interfacial region. Supercapacitors are currently a prominent area of research for energy storage devices as they have high power density, long cycling life, and short charging time [2-4]. Moreover, they have higher energy density than conventional dielectric capacitors [1,4]. Supercapacitors can be used either alone as a primary power source or as an auxiliary one with rechargeable batteries for high-power applications, such as industrial mobile equipment and hybrid/electric vehicles.

Electrochemical capacitors can be further divided into two categories based on energy storage modes, that is, electrical double layer capacitors and redox or pseudocapacitors. In the former, charge separation takes place on either side of the interface leading to the formation of an electrochemical double layer. When a voltage is applied, a current is generated due to the rearrangement of charges [5,6]. Pseudocapacitors, in contrast, get

their charge from the fast and reversible reduction and oxidation (redox) reaction that takes place at the electrode-electrolyte interface due to change in oxidation state [7-9]. These pseudocapacitors are characterized by superior capacitance compared to their double-layer counterparts [10].

A number of inorganic materials have been shown in the past to exhibit outstanding capacitor characteristics; among them, hydrous RuO₂ showed the best performance, but its high cost limits its application as a supercapacitor [11,12]. Thus, the focus of the current research is being placed on low-cost materials such as NiO [13,14], MnO₂ [15], Ni(OH)₂ [16], Co₃O₄ [17], and V₂O₅ [18].

NiO-based nanostructures and thin films have been extensively applied as electrode materials for lithium-ion batteries and fuel cells [19-21], electrochromic films [22,23], gas sensors [24], and electrochemical supercapacitors [22,25]. Because NiO is cheaper than RuO₂, environmentally benign, and easy to process using a variety of methods, it deserved, and continue to deserve, considerable research activities toward high-performance electrochemical supercapacitor applications [13,14,22,25,26].

* Correspondence: mohammed.es-souni@fh-kiel.de
Institute for Materials and Surface Technology (IMST), University of Applied Sciences Kiel, Kiel 24149, Germany

A large specific surface area in redox energy storage supercapacitors ensures an efficient contact with more electroactive sites even at high current densities [26,27]. Efficient electrode-electrolyte contact also depends upon the kind of nanostructures and porosity [26,27]. Because the rate capability (charge–discharge) of the electrode materials is mainly determined by ion diffusion kinetics and electronic conductivity [28], nano/micro hierarchical porous superstructures are best suited as electrode materials in energy storage devices, especially one-dimensional (1D) nanostructures which provide short transport pathways for electrons and ions [29,30]. High-aspect-ratio and high-surface-area nanostructures provide easy diffusion paths and improved diffusivity, which is crucial for better performance, while low-aspect-ratio nanostructures provide good mechanical stability [31]. Thus, morphology plays a vital role in defining the performance of the supercapacitor electrode.

In the present work, we take advantage of anodized alumina (AAO) templates to process 1D NiO nanostructures starting from Ni nanotubes (NTs) that are oxidized to yield 1D NiO nanostructures. By judicious choice of annealing temperature and time, the morphology of NiO could be tuned from NTs to nanorods (NRs), thus allowing the investigation of morphological effects on energy storage capability. The results indeed show that NiO NTs are characterized by superior capacitance performance characteristics in comparison to NiO NRs.

Methods

The following chemicals were used as purchased: nickel chloride ($\text{NiCl}_2 \cdot 6\text{H}_2\text{O}$), nickel sulfate ($\text{NiSO}_4 \cdot 7\text{H}_2\text{O}$), and boric acid (H_3BO_3) (Sigma-Aldrich, Munich, Germany) and NaOH (Roth, Karlsruhe, Germany). All the chemicals were of analytical grade purity. Deionized water was used to prepare aqueous solutions ($\geq 18 \text{ M}\Omega$). Commercial AAO templates (60 μm thick) were obtained from Whatman International (Kent, UK) with 200-nm pore size (although the actual pore size ranges from 220 to 280 nm). The electrochemical experiments were performed at room temperature in a standard three-electrode cell. The electrodeposition and cyclic voltammograms (CVs) were made using an electrochemical workstation (ZAHNER IM6e, Kronach, Germany), and charging-discharging tests were performed using Source Meter 2400 (Keithley, Cleveland, OH, USA). A Pt mesh and hydroflex (H_2 reference electrode) were used as counter and reference electrodes, respectively. All potentials are referred to the standard hydrogen electrode (SHE).

The microstructure and morphology of the nanostructures were characterized with a high-resolution scanning electron microscope (Ultra Plus, Zeiss, Oberkochen, Germany). X-ray diffraction (X'Pert Pro system, PANalytical, Almelo, The Netherlands) data was obtained in grazing incident geometry

with fixed angles of 1.5° and 0.05° step using monochromatic Cu $K\alpha$ radiation ($\lambda = 1.5418 \text{ \AA}$). The process steps for preparing the nanostructures were detailed in our previous paper [32] and are described briefly below.

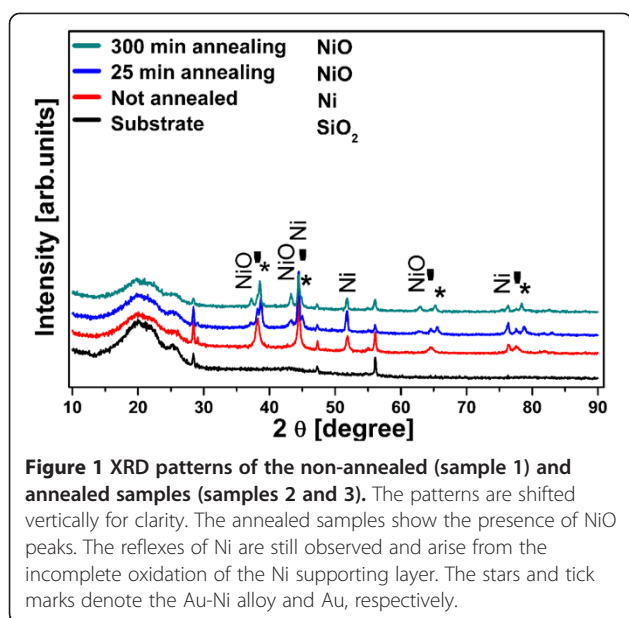
One side of the AAO template was sputtered with 20-nm gold (Au) to make it conductive. Subsequently, a thin Ni layer was electroplated from an electrolyte containing 310 g/L $\text{NiSO}_4 \cdot 7\text{H}_2\text{O}$, 50 g/L $\text{NiCl}_2 \cdot 6\text{H}_2\text{O}$, and 40 g/L H_3BO_3 on the sputtered Au to close the AAO template completely. The supporting Ni layer was 350 nm thick. Then Ni nanotubes (Ni NTs) were grown electrochemically via a bottom-up approach from the same electrolyte (310 g/L $\text{NiSO}_4 \cdot 7\text{H}_2\text{O}$, 50 g/L $\text{NiCl}_2 \cdot 6\text{H}_2\text{O}$, and 40 g/L H_3BO_3) under potentiostatic conditions at -0.9 V for 50 s. These AAO templates containing Ni NT were washed several times with distilled water and dried in air. Several Ni NT samples were prepared by the procedure described above, and out of these three cracks, free samples (samples 1, 2, and 3) were selected for electrochemical experiments.

Sample 1 was not annealed while samples 2 and 3 were annealed in air within the AAO template from room temperature to 450°C (heating rate 400 K/h) and were kept at this temperature for 25 min (sample 2) and 300 min (sample 3), respectively. These annealed samples were taken out of the furnace and cooled down in air. All the three samples were glued with (non-conductive) double-sided adhesion tape to the SiO_2 supporting substrate, before dissolving the AAO template with 5% NaOH. To estimate the maximum contribution of the supporting Ni layer to capacitance, a Ni film sample was prepared by electrodeposition Ni on an Au-sputtered SiO_2 substrate under the same electrodeposition conditions and annealed at 450°C .

To measure the pseudocapacitance of the electrodes, CVs were recorded in an aqueous electrolyte containing 1 M KOH between 0.35 and 0.850 V at different scan rates. The charge–discharge behavior at different current densities and long-term cycling stability were tested in 1 M KOH. Before each electrochemical experiment, N_2 was bubbled in the electrolyte for 15 min. The electrochemical experiments were conducted on a minimum of three to five samples each.

Results and discussion

The X-ray diffraction (XRD) patterns of the Ni (non-annealed sample 1) and NiO (annealed samples 2 and 3) nanostructures obtained under the deposition and annealing conditions described above are displayed in Figure 1. For the NiO nanostructures (samples 2 and 3), the NiO (cubic, NaCl structure) peaks become more distinguishable with increased annealing time. This is due to increasing oxide thickness along with enhanced crystal orientation. Using the Scherrer equation and the



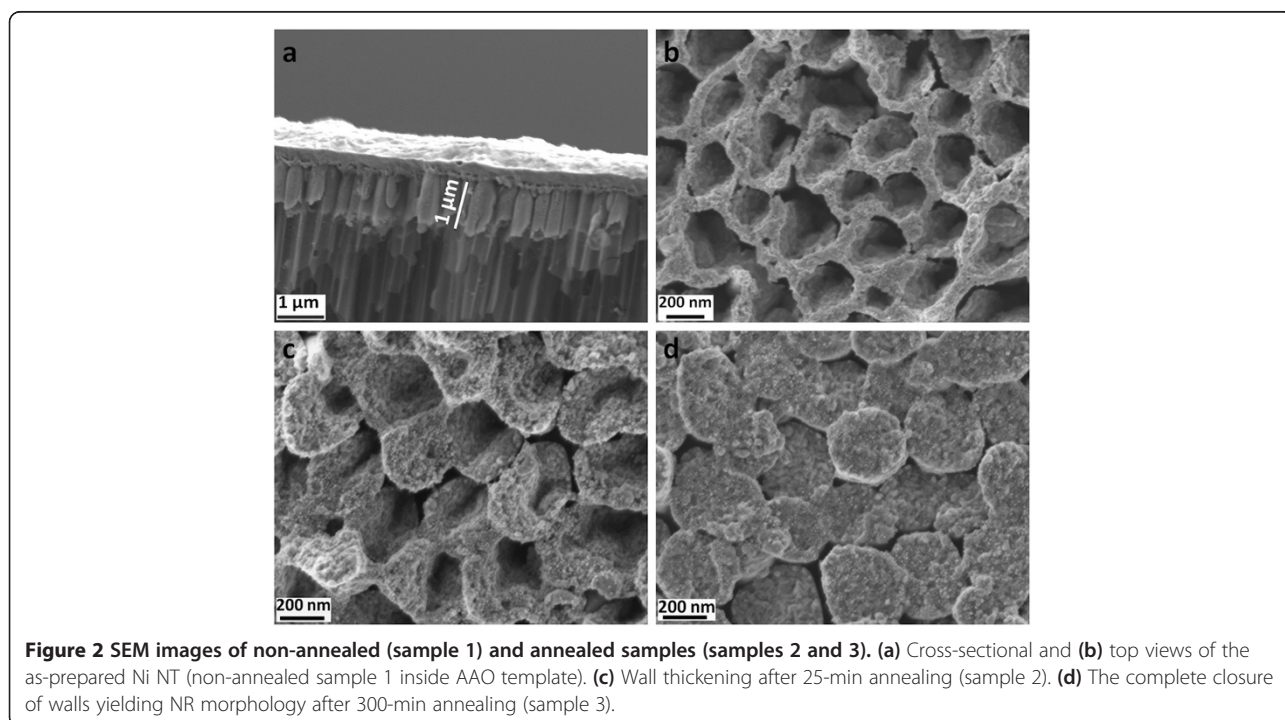
(200) reflection at 43.3° , the mean grain size calculated for sample 2 is 12.8 and that for sample 3 is 19.4 nm. The peaks indicated by a star (*) correspond to a Au-Ni binary alloy which is formed at this annealing temperature (450°C) due to the presence of sputtered Au. The chemical composition of this alloy was estimated from the peak positions, applying Vegard's law and using the lattice constants of $a = 4.0789 \text{ \AA}$ for Au and $a = 3.5238 \text{ \AA}$ for Ni. According to it, the Au-Ni

alloy is composed of 90 at.% Au and 10 at.% Ni for the 25-min-annealed sample and 93 at.% Au and 7 at.% Ni for the 300-min-annealed samples.

From the above, it can be seen that metallic Ni still dominates the XRD spectrum, and it appears necessary to estimate the magnitude of oxidation of the nanostructures. For doing this, we make use of the data published in [33] which shows that Ni oxidation follows a parabolic law in a wide range of temperature. Through extrapolation and taking into account the surface area of the 1D morphology involved (see calculation details in Additional file 1: S1), it can be shown that sample 2 consists of 60% NiO while sample 3 is completely oxidized. Using the same procedure, only a small fraction of oxide (0.37%) is calculated for the underlying Ni layer, which explains the dominance of the Ni peaks in the XRD patterns.

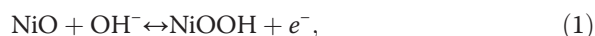
The morphology of the nanostructures obtained is shown in Figure 2. The non-annealed sample 1 (Figure 2a, b) shows solely Ni NTs that form via nucleation and growth at the pore walls because of the presence of an extremely thin Au layer (see the experimental section and our previous paper [32]). The judicious deposition time for Ni to obtain NT is 50 s.

During annealing, the oxide layer nucleates and grows from the exposed inside walls and thickens in the direction of the inner-tube diameter. This suggests an outward diffusion of the Ni species toward oxygen ions. On the non-exposed outside walls that are confined by the AAO template, no oxide growth is expected. A short

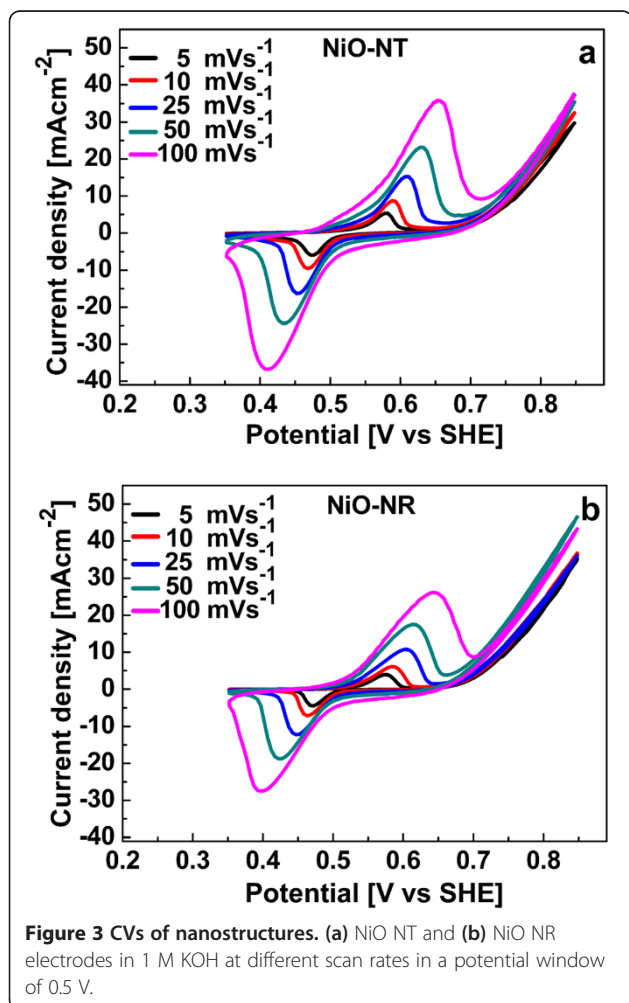


annealing time leads to incomplete oxidation of the Ni NTs, resulting in the formation of an oxide scale supported on a remaining Ni layer (see also the XRD results above and Additional file 1: S1). This is the case of sample 2 (Figure 2c; 25-min annealing). For longer annealing time, complete closure of the NT, to finally give the NR morphology as shown in Figure 2d, is achieved because of the volume increase associated with NiO oxide formation. This is the case of sample 3 (300-min annealing).

Figure 3 shows the CV curves of the NiO NTs and NiO NRs recorded using a potential window of 0.5 V (between 0.35 and 0.85 V) at various scan rates (5, 10, 25, 50, and 100 mV/s). The two strong peaks observed in the anodic and cathodic directions correspond to the faradic redox reaction, expressed as follows [34,35]:



involving ionic and electronic transport at the NiO/electrolyte interface.



The shapes of the anodic and cathodic curves are similar for all scan rates. The profile of the CVs implies that the redox reaction at the interface of the nanostructure is reversible [36]. The peak current density increases with the scan rate because the redox reaction is diffusion-limited, and at a higher scan rate, the interfacial reaction kinetics and transport rate are not efficient enough. According to Equation 1, anions are exchanged with the electrolyte and electrode interface during redox reaction. This ion transfer process is slow and rate limiting, and higher scan rates are associated with smaller diffusion layer thickness [37]. This means that less of the electrode surface is utilized which lowers the resistivity and increases the current density that is also an indication of the pseudocapacitive behavior of the NiO nanostructures [36]. Further, the anodic and cathodic peaks are shifted to higher and lower potentials, respectively, with increasing scan rates (Figure 3). It again indicates that the ionic diffusion rate is not fast enough to keep pace with electronic neutralization in the redox reaction [38].

The specific capacitances were calculated from the CVs using the equation given below [39,40]:

$$C = \frac{I}{2 \cdot V \cdot S \cdot m}, \quad (2)$$

where C is the specific capacitance (F/g), I the integrated area (V A) of the CV curve in one complete cycle, V the potential window (V), S the scan rate (V/s), and m the mass (g) of NiO, calculated using the oxidized Ni mass% outlined above, i.e., 60% and 100% for the NT and NR, respectively (Additional file 1: S1).

The dependence of the capacitance on the scan rate is depicted in Figure 4 and shows the downward trend with increasing scan rate discussed above. The error bars correspond to the standard deviation in mass, which is

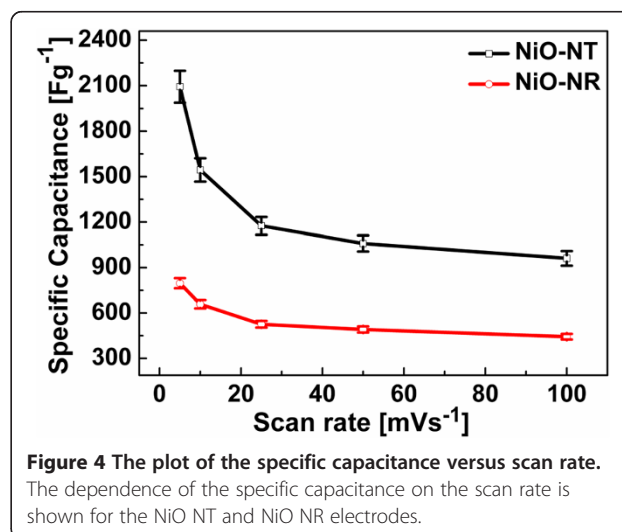


Table 1 Comparison of specific capacitances of different NiO nanostructures

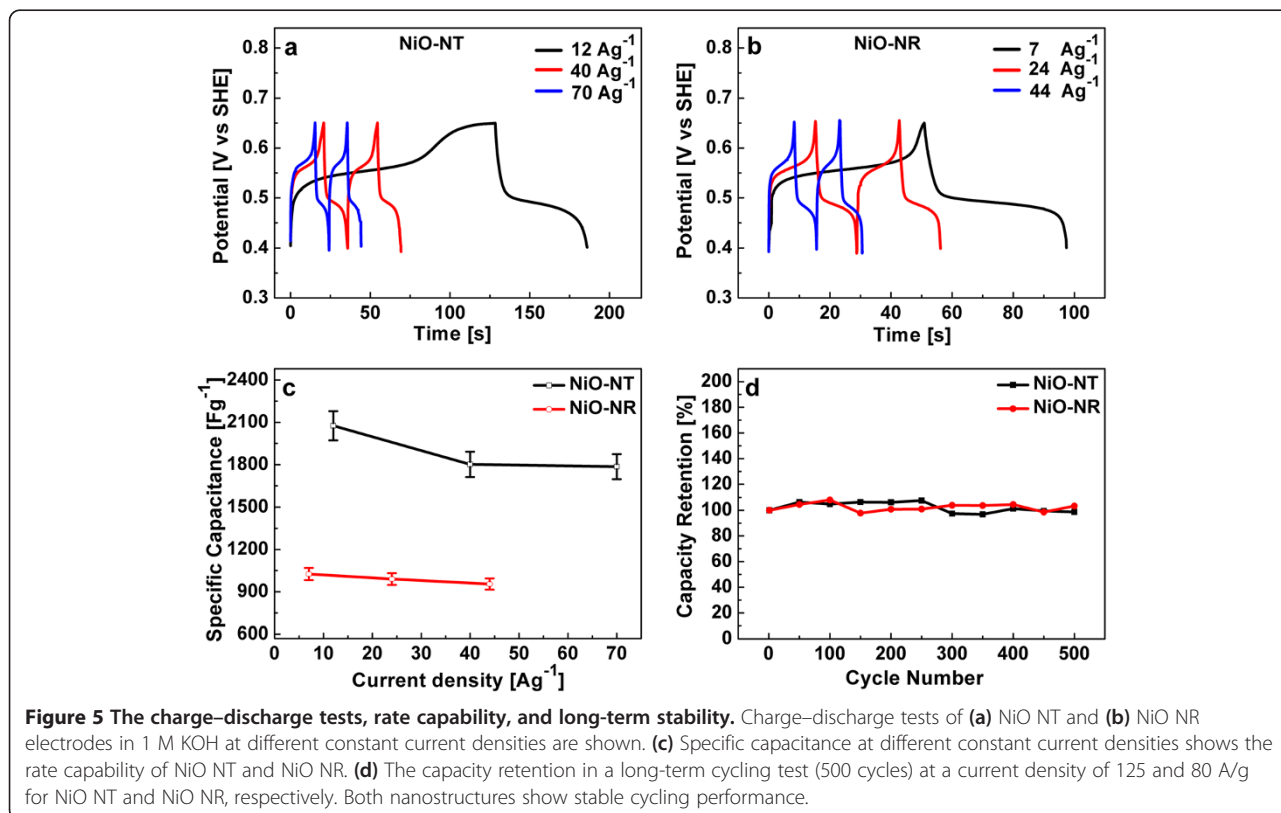
Scan rate (mV/s)	Specific capacitance (F/g)		
	NiO NR	NiO NT	NiO-nanoporous film [14]
5	797	2,093	1,208
10	658	1,544	940
25	526	1,175	748
50	491	1,059	590
100	443	961	417

The NiO NT and NiO NR prepared in our work are compared with one of the recent works from the literature [14].

5% (0.935 μg) and 4.2% (0.854 μg) for NiO NTs and NiO NRs, respectively.

Table 1 highlights the specific capacitances of our nanostructures and compares them with one of the recent works from the literature [14] at similar conditions of scan rates and electrolyte concentrations (1 M KOH). The specific values are for the capacitance obtained at slower scan rate because it represents nearly the full utilization of the electrode [41] through better ion penetration that is diffusion-limited [42]. Table 1 shows that the NiO NT sample is characterized by the highest specific capacitance (mean value of 2,093 F/g at 5 mV/s) while the NiO NR sample falls lower than the specific

capacitance reported for NiO nanoporous films [14], except at 100 mV/s. The specific capacitance of the NiO NT sample is the highest ever reported for NiO nanostructures and approaches the theoretical value of approximately 2,584 F/g [43]. This is ascribed to the nanocrystalline nature of NiO grown in this work and the high surface area offered by the 1D NT nanostructure which ensures efficient contact with the electrolyte. We do not expect any contribution from NiO of the supporting layer for two reasons: firstly, only a negligible fraction of the Ni supporting layer is oxidized because the exposed area is very small due to the high density of the nanostructure, including the AAO template; secondly, even in the presence of an oxide layer, most of its area is occupied by the nanostructures and the effective exposed area (to the electrolyte) of the supporting layer is very small considering the average diameter (250 nm) and density ($1 \times 10^9 \text{ cm}^{-2}$) of the nanostructures. The maximum contribution of the underlying supporting NiO film was independently assessed on a plain Ni film of the same thickness, oxidized under the same conditions as above. The maximum capacitance was found to be 223 F/g at 5 mV/s scan rate (Additional file 1: Figure S2). This value of specific capacitance is for the fully utilized surface of the NiO film. This allows us to conclude that the capacitances measured reflect solely the contribution of our 1D nanostructures.



The galvanostatic charging-discharging tests were performed at different constant current densities and are displayed in Figure 5a, b. The charge-discharge curves are non-linear with current density for both NiO nanostructures, as a further indication of their pseudocapacitive behavior [9].

From these charge-discharge curves, the specific capacitance was calculated at different current densities using the following equation:

$$C = \frac{I \cdot t}{V \cdot m}, \quad (3)$$

where C is the specific capacitance, I the current (A), t the discharge time (s), m the mass of NiO (g), and V the potential window (V). Figure 5c shows the specific capacitance as a function of current densities, which is the measure of the rate capability [44]. The specific capacitances of NiO NT are 2,076, 1,801, and 1,786 F/g at 12, 40, and 70 A/g, respectively, which demonstrates the unusually high power density obtained at high discharge current densities: 86% of capacitance is retained at the discharge current density of 70 A/g. The specific capacitances for NiO NR are 1,026, 990, and 955 F/g at 7, 24, and 44 A/g, respectively, which implies that the NiO NR structure retains 93% of its capacitance.

The long-term stability against cyclic charging-discharging is another important property of a capacitor structure. Figure 5d shows the long-term cycling performance of both NiO nanostructures at a constant current density of 125 and 80 A/g for NiO NT and NiO NR, respectively. Capacity retention over 500 cycles is almost 100% for both NiO nanostructures. The properties obtained for our nanostructures are outstanding in all aspects regarding supercapacitor performance. The NiO NT structure surpasses the results published so far on NiO supercapacitors; the maximum specific capacitance values (at constant current densities) achieved for NiO nanostructures of different morphologies, e.g., nanofibers [45], nanoflowers [46], nanoflakes [13], porous structures [47], nanoporous films [14], and nanorod arrays [48], span the range between 336 and 2,018 F/g (the latter value has been reported for NiO NR arrays on Ni foam at the fairly low current density of 2.2 F/g and is largely different from the value obtained for our NiO NR because of different structural dimensions). As outlined above, the nanocrystalline grain size together with the high surface area of the tubular structure is responsible for the high performance of the NiO NT structure that ensures an intimate contact with the electrolyte, i.e., offering a large density of active sites for OH⁻ ions for the redox reaction. Furthermore, the robustness and chemical stability of the nanostructures reported here are responsible for their stability against cyclic charging-discharging.

Conclusions

One-dimensional NiO nanostructures for energy storage applications are processed using a combination of AAO-aided template synthesis and annealing treatments. The judicious selection of annealing time and temperature enabled us to control the morphology of the NiO nanostructures, from nanotubes to nanorods. Our electrochemical capacitance results show a large dependence of capacitance on morphology of the nanostructures. Particularly, the NiO NT structure shows outstanding capacitance properties with a capacitance value that surpasses those published so far in the literature for different NiO nanostructures. Beyond the achieved high capacitance value, the rate capability (charge-discharge capacitance at high current density) is also outstanding. Concerning the long-term stability on cyclic charging-discharging, full capacity retention is achieved for both nanostructures over 500 cycles.

Additional file

Additional file 1: Magnitude of oxidation and specific capacitance of the NiO film. Magnitude of oxidation (S1): interpolation of experimental data from the literature to calculate the parabolic rate constant Log K_p (Figure S1) and calculation of weight gain per unit area M (Table S1). Specific capacitance of NiO-Film (S2): the specific capacitance of the supporting NiO film is measured at different scan rates (Figure S2) to estimate the maximum contribution of the supporting NiO film.

Competing interests

The authors declare that they have no competing interests.

Authors' contributions

FID carried out the synthesis and characterization. KRM improved the manuscript and participated in the studies. MES conceived, planned, and directed the research and made final corrections to the manuscript. All authors read and approved the final manuscript.

Acknowledgements

Financial support of this work is provided by the European Commission, INTERREG IVA, Southern Denmark-Schleswig-K.E.R.N, Project#111-1.2-12.

Received: 7 August 2013 Accepted: 15 August 2013

Published: 23 August 2013

References

1. Winter M, Brodd RJ: What are batteries, fuel cells, and supercapacitors? *Chem Rev* 2004, **104**:4245-4270.
2. Kuperman A, Aharon I: Battery-ultracapacitor hybrids for pulsed current loads: a review. *Renewable Sustainable Energy Rev.* 2011, **15**:981-992.
3. Miller JR, Simon P: Electrochemical capacitors for energy management. *Science* 2008, **321**:651-652.
4. Simon P, Gogotsi Y: Materials for electrochemical capacitors. *Nat Mater* 2008, **7**:845-854.
5. Lota G, Centeno TA, Frackowiak E, Stoeckli F: Improvement of the structural and chemical properties of a commercial activated carbon for its application in electrochemical capacitors. *Electrochim Acta* 2008, **53**:2210-2216.
6. Fang B, Binder L: A modified activated carbon aerogel for high-energy storage in electric double layer capacitors. *J Power Sources* 2006, **163**:616-622.
7. Conway BE: Transition from "supercapacitor" to "battery" behavior in electrochemical energy storage. *J Electrochem Soc* 1991, **138**:1539-1548.

8. Sarangapani S, Tilak BV, Chen C-P: **Materials for electrochemical capacitors theoretical and experimental constraints.** *J Electrochem Soc* 1996, **143**:3791–3799.
9. Conway BE: *Electrochemical Supercapacitors: Scientific Fundamentals and Technological Applications.* New York: Plenum; 1999.
10. Zheng JP, Cygan PJ, Jow TR: **Hydrous ruthenium oxide as an electrode material for electrochemical capacitors.** *J Electrochem Soc* 1995, **142**:2699–2703.
11. Ke YF, Tsai DS, Huang YS: **Electrochemical capacitors of RuO₂ nanophase grown on LiNbO₃(100) and sapphire(0001) substrates.** *J Mater Chem* 2005, **15**:2122–2127.
12. Zheng JP, Jow TR: **A new charge storage mechanism for electrochemical capacitors.** *J Electrochem Soc* 1995, **142**:L6–L8.
13. Lang JW, Kong LB, Wu WJ, Luo YC, Kang L: **Facile approach to prepare loose-packed NiO nano-flakes materials for supercapacitors.** *Chem Commun* 2008:4213–4215. doi:10.1039/B800264A.
14. Liang K, Tang X, Hu W: **High-performance three-dimensional nanoporous NiO film as a supercapacitor electrode.** *J Mater Chem* 2012, **22**:11062–11067.
15. Fisher AE, Pettigrew KA, Rolison DR, Stround RM, Long JW: **Incorporation of homogeneous, nanoscale MnO₂ within ultraporous carbon structures via self-limiting electroless deposition: implications for electrochemical capacitors.** *Nano Lett* 2007, **7**:281–286.
16. Patil UM, Gurav KV, Fulari VJ, Lokhande CD, Joo OS: **Characterization of honeycomb like “β-Ni(OH)₂” thin films synthesized by chemical bath deposition method (CBD) and their supercapacitor application.** *J Power Sources* 2009, **188**:338–342.
17. Zheng MB, Cao J, Liao ST, Liu JS, Chen HQ, Zhao Y, Dai WJ, Ji GB, Cao JM, Tao J: **Preparation of mesoporous Co₃O₄ nanoparticles via solid–liquid route and effects of calcination temperature and textural parameters on their electrochemical capacitive behaviors.** *J Phys Chem C* 2009, **113**:3887–3894.
18. Lee HY, Goodenough JB: **Ideal supercapacitor behavior of amorphous V₂O₅·nH₂O in potassium chloride (KCl) aqueous solution.** *J Solid State Chem* 1999, **148**:81–84.
19. Poizot P, Laruelle S, Grugeon S, Dupont L, Tarascon JM: **Nano-sized transition-metal oxides as negative-electrode materials for lithium-ion batteries.** *Nature* 2000, **407**:496–499.
20. Mamak M, Coombs N, Ozin GA: **Mesoporous nickel–yttria–zirconia fuel cell materials.** *Chem Mater* 2001, **13**:3564–3570.
21. Wang X, Song J, Gao L, Jin J, Zheng H, Zhang Z: **Optical and electrochemical properties of nanosized NiO via thermal decomposition of nickel oxalate nanofibres.** *Nanotechnology* 2005, **16**:37–39.
22. Karlsson J, Roos A: **Angle-resolved optical characterisation of an electrochromic device.** *Sol Energy* 2000, **68**:493–497.
23. Fantini MCA, Ferreira FF, Gorenstein A: **Theoretical and experimental results on Au-NiO and Au-CoO electrochromic composite films.** *Solid State Ion* 2002, **152**:867–872.
24. Makiak E, Opilaski Z: **Transition metal oxides covered Pd film for optical H₂ gas detection.** *Thin Solid Films* 2007, **515**:8351–8355.
25. Miller EL, Rocheleau RE: **Electrochemical behavior of reactively sputtered iron-doped nickel oxide.** *J Electrochem Soc* 1997, **144**:3072–3077.
26. Xiong S, Yuan C, Zhang X, Qian Y: **Mesoporous NiO with various hierarchical nanostructures by quasi-nanotubes/nanowires/nanorods self-assembly: controllable preparation and application in supercapacitors.** *CrystEngComm* 2011, **13**:626–632.
27. Wang DW, Li F, Cheng HM: **Hierarchical porous nickel oxide and carbon as electrode materials for asymmetric supercapacitor.** *J Power Sources* 2008, **185**:1563–1568.
28. Hou Y, Cheng YW, Hobson T, Liu J: **Design and synthesis of hierarchical MnO₂ nanospheres/carbon nanotubes/conducting polymer ternary composite for high performance electrochemical electrodes.** *Nano Lett* 2010, **10**:2727–2733.
29. Jiang H, Zhao T, Ma J, Yan CY, Li CZ: **Ultrafine manganese dioxide nanowire network for high-performance supercapacitors.** *Chem Commun* 2011, **47**:1264–1266.
30. Reddy ALM, Shaijumon MM, Gowda SR, Ajayan PM: **Coaxial MnO₂/carbon nanotube array electrodes for high-performance lithium batteries.** *Nano Lett* 2009, **9**:1002–1006.
31. Guo YG, Hu JS, Wan LJ: **Nanostructured materials for electrochemical energy conversion and storage devices.** *Adv Mater* 2008, **20**:2878–2887.
32. Dar FI, Habouti S, Minch R, Dietze M, Es-Souni M: **Morphology control of 1D noble metal nano/heterostructures towards multi-functionality.** *J Mater Chem* 2012, **22**:8671–8679.
33. Zima GE: *Some high temperature oxidation characteristics of nickel with chromium additions.* Pasadena: Office of Naval Research (US Government); Seventh technical report. Contract No. N6onr-24430; 1956.
34. Srinivasan V, Weidner JW: **An electrochemical route for making porous nickel oxide electrochemical capacitors.** *J Electrochem Soc* 1997, **144**:L210–L213.
35. Nam KW, Yoon WS, Kim KB: **X-ray absorption spectroscopy studies of nickel oxide thin film electrodes for supercapacitors.** *Electrochim Acta* 2002, **47**:3201–3209.
36. Kim JH, Zhu K, Yan Y, Perkins CL, Frank AJ: **Microstructure and pseudocapacitive properties of electrodes constructed of oriented NiO-TiO₂ nanotube arrays.** *Nano Lett* 2010, **10**:4099–4104.
37. Compton RG, Banks CE: **Cyclic voltammetry at macroelectrodes.** In *Understanding Voltammetry.* Singapore: World Scientific; 2007:111–120.
38. Li X, Xiong S, Li J, Bai J, Qian Y: **Mesoporous NiO ultrathin nanowire networks topotactically transformed from α-Ni(OH)₂ hierarchical microspheres and their superior electrochemical capacitance properties and excellent capability for water treatment.** *J Mater Chem* 2012, **22**:14276–14283.
39. Nam KW, Kim KB: **A study of the preparation of NiO_x electrode via electrochemical route for supercapacitor applications and their charge storage mechanism.** *J Electrochem Soc* 2002, **149**:A346–A354.
40. Pang SC, Anderson MA, Chapman TW: **Novel electrode materials for thin-film ultracapacitors: comparison of electrochemical properties of sol-gel-derived and electrodeposited manganese dioxide.** *J Electrochem Soc* 2000, **147**:444–450.
41. Patil UM, Salunkhe RR, Gurav KV, Lokhande CD: **Chemically deposited nanocrystalline NiO thin films for supercapacitor application.** *Appl Surf Sci* 2008, **255**:2603–2607.
42. Huggins RA: **Supercapacitors and electrochemical pulse sources.** *Sol Stat Ionics* 2000, **134**:179–195.
43. Kong DS, Wang JM, Shao HB, Zhang JQ, Cao CN: **Electrochemical fabrication of a porous nanostructured nickel hydroxide film electrode with superior pseudocapacitive performance.** *J Alloys Compd* 2011, **509**:5611–5616.
44. Zhou R, Meng C, Zhu F, Li Q, Liu C, Fan S, Jiang K: **High-performance supercapacitors using a nanoporous current collector made from super-aligned carbon nanotubes.** *Nanotechnology* 2010, **21**:345701.
45. Ren B, Fan M, Liu Q, Wang J, Song D, Bai X: **Hollow NiO nanofibres modified by citric acid and the performances as supercapacitor electrode.** *Electrochim Acta* 2013, **92**:197–204.
46. Kim S-I, Lee J-S, Ahn H-J, Song H-K, Jang J-H: **Facile route to an efficient NiO supercapacitor with a three-dimensional nanonetwork morphology.** *Appl Mater Interfaces* 2013, **5**:1596–1603.
47. Liu M, Chang J, Sun J, Gao L: **Synthesis of porous NiO using NaBH₄ dissolved in ethylene glycol as precipitant for high-performance supercapacitor.** *Electrochim Acta* 2013, **107**:9–15.
48. Lu Z, Chang Z, Liu J, Sun X: **Stable ultrahigh specific capacitance of NiO nanorod arrays.** *Nano research* 2011, **4**:658–665.

doi:10.1186/1556-276X-8-363

Cite this article as: Dar et al: Morphology and property control of NiO nanostructures for supercapacitor applications. *Nanoscale Research Letters* 2013 **8**:363.